

Water uptake in biochars: The roles of porosity and hydrophobicity

The Faculty of Oregon State University has made this article openly available.
Please share how this access benefits you. Your story matters.

Citation	Gray, M., Johnson, M. G., Dragila, M. I., & Kleber, M. (2014). Water uptake in biochars: The roles of porosity and hydrophobicity. <i>Biomass and Bioenergy</i> , 61, 196-205. doi:10.1016/j.biombioe.2013.12.010
DOI	10.1016/j.biombioe.2013.12.010
Publisher	Elsevier
Version	Version of Record
Citable Link	http://hdl.handle.net/1957/47480
Terms of Use	http://cdss.library.oregonstate.edu/sa-termsfuse

Available online at www.sciencedirect.com

ScienceDirect

<http://www.elsevier.com/locate/biombioe>

Water uptake in biochars: The roles of porosity and hydrophobicity

Myles Gray^{a,*}, Mark G. Johnson^b, Maria I. Dragila^a, Markus Kleber^{a,c}

^a Oregon State University, Department of Crop and Soil Science, 3017 Ag and Life Sciences Bldg., Oregon State University, Corvallis, OR 97331, USA

^b U.S. Environmental Protection Agency, Western Ecology Division, 200 SW 35th St., Corvallis, OR 97333, USA

^c Institute of Soil Landscape Research, Leibniz-Center for Agricultural Landscape Research (ZALF), 15374 Müncheberg, Germany

ARTICLE INFO

Article history:

Received 21 August 2013

Received in revised form

10 December 2013

Accepted 17 December 2013

Available online 23 January 2014

Keywords:

Biochar

Water uptake

Porosity

Hydrophobicity

FTIR

ABSTRACT

We assessed the effects of porosity and hydrophobicity on water uptake by biochars. Biochars were produced from two feedstocks (hazelnut shells and Douglas fir chips) at three production temperatures (370 °C, 500 °C, and 620 °C). To distinguish the effects of porosity from the effects of hydrophobicity, we compared uptake of water to uptake of ethanol (which is completely wetting and not affected by hydrophobic materials). For both feedstocks, low temperature biochars took up less water than high temperature biochars but the same amount of ethanol, suggesting that differences in water uptake based on production temperature reflect differences in surface hydrophobicity, not porosity. Conversely, Douglas fir biochars took up more water than hazelnut shell biochars due to greater porosity. Thus, designing biochars for water holding applications requires two considerations: (a) creating sufficient porosity through feedstock selection, and (b) determining a production temperature that reduces hydrophobicity to an acceptable level.

© 2013 Elsevier Ltd. All rights reserved.

1. Introduction

Biochars are carbon-rich solids produced by heating biomass in the absence of oxygen - a process known as pyrolysis. Pyrolysis occurs naturally during forest and grassland fires, as evidenced by the presence of a charcoal residue. Recently, industrial production of biochar has become part of a strategy to simultaneously produce renewable bioenergy, remove carbon from the atmosphere, and produce environmentally beneficial products from biomass [1]. During pyrolysis, between 50% and 80% of biomass is converted into combustible liquids and vapors, which can be used to produce bioenergy [2]. The remaining biomass is converted into biochar, which

retains some residual feedstock properties but is essentially composed of amorphous carbon, turbostratic crystallites of polycondensed aromatic sheets, and interspersed voids [3,4]. Biochars tend to decompose slowly in the environment and are thus considered temporal sinks for atmospheric CO₂ [5]. Feedstock selection and pyrolysis conditions affect biochar properties [6–8]. By understanding and controlling these factors it is possible to create value-added “designer biochars” for specific environmental applications such as soil improvement [9] and removal of heavy metals [10] and organic contaminants from water [11].

Biochars can be considered porous media. Typically, biochar porosity has been classified following IUPAC conventions by distinguishing between micropores (<2 nm), mesopores

* Corresponding author. Tel.: +1 541 250 2250.

E-mail address: myles.gray@oregonstate.edu (M. Gray).

0961-9534/\$ – see front matter © 2013 Elsevier Ltd. All rights reserved.

<http://dx.doi.org/10.1016/j.biombioe.2013.12.010>

(2–50 nm), and macropores (>50 nm) [12]. This classification system has been widely used with gas adsorption to assess porosity of activated carbons, but does not adequately describe larger biochar pore sizes that may dominate water retention. Here we propose a functional biochar pore size classification system consisting of: 1) external pores, being pores between biochar particles, 2) residual macropores, being internal pores inherited from feedstock structure, with a pore size distribution centered in the low micrometer range, and 3) pyrogenic nanopores, being internal pores produced at higher production temperatures, with a pore size distribution in the low nanometer range. The size and shape of external pores depend on particle size, particle morphology, and media compaction. Residual macropores tend to be between 1 and 100 μm in diameter (Fig. S-1), depending on feedstock and have been investigated extensively using scanning electron microscopy [13]. These pores are inherited from plant cellular structures [14] with sizes in the range relevant to ecological and hydrological processes, and are thought to contain the majority of biochar pore volume [15]. Pyrogenic nanopores are voids that form within the carbon structure as a result of chemical changes during pyrolysis and are more prevalent in higher production temperature biochars [3]. These pores are generally smaller than 50 nm (Fig. S-1), with the vast majority being smaller than 2 nm [16,17]. Pyrogenic nanopores comprise the majority of biochar surface area [18,19], and thus provide the most sites for adsorption of nutrients and contaminants from aqueous streams [7,19].

Understanding water uptake in biochars is critical to produce effective products, and while some research has quantified the effect of biochar on water holding capacity in soils [20], little research has focused specifically on water uptake in biochars. Water uptake in porous media depends on capillary forces, which can act to enable or prevent water entry into pores. The strength of capillary forces depends on surface chemistry and physical properties of the media, and is frequently described by the Laplace equation:

$$P_c = \frac{2\gamma \cos \theta}{r} \quad (1)$$

where P_c is the differential capillary pressure across the liquid–gas interface (N m^{-2}); γ is the surface tension of water (N m^{-1}); θ is the contact angle of water, which depends on interfacial energies and thus biochar surface chemistry; and r is the pore radius (m). Capillary pressure forces can be positive or negative depending on surface properties: hydrophilic surfaces with contact angles less than 90° generate positive capillary pressures, driving water into pores, while hydrophobic surfaces with contact angles greater than 90° generate negative capillary pressures, preventing water from entering pores. The magnitude of positive or negative capillary pressure is inversely proportional to pore radius. Of particular concern is the presence of hydrophobic surfaces in pores with radii in the order of micrometers and nanometers, which can generate strong negative capillary pressures that prevent water entry into pores.

Total water uptake of biochar media depends both on capillary forces as well as total porosity, which represents the media's theoretical maximum available water holding capacity. Depending on feedstock selection and production

conditions, biochars exhibit large ranges in porosity [13,14,21] and surface chemistry [7,22]. The goal of the work presented here is to determine how these properties interact to control total water uptake by biochar. To achieve this goal, we investigated (a) the processes and factors that control the total pore volume available for water storage, and (b) the mechanisms that allow or prevent water entry into biochar pore space. Our approach consisted of thorough physical and surface chemical characterization combined with an experiment designed to distinguish porosity effects from surface chemistry effects. This involved the development and testing of four hypotheses.

Given that feedstock selection and pyrolysis temperature are known to affect physical and chemical biochar properties, we hypothesized that (1) biochars produced from different feedstocks would exhibit different water uptake characteristics and (2) water uptake would vary as a function of pyrolysis temperature within each feedstock. To differentiate between mechanisms responsible for variations in water uptake, we compared water and ethanol uptake dynamics in the same samples. Final ethanol uptake values were considered proxies for total porosity due to the fact that ethanol is assumed to be a completely wetting fluid, exhibiting a contact angle of zero degrees on most surfaces [23], and because both oxygen [24] and nitrogen [25] are relatively soluble in ethanol, minimizing the effects of pore air pressure during imbibition. We hypothesized (3) that this procedure would allow assessment of the relative importance of hydrophobicity (which reduces water uptake but not ethanol uptake) versus total porosity (which had the same effect for both water uptake and ethanol uptake). Finally, we investigated whether exposure to saturated water vapor could be used as a simple post-production treatment to increase water uptake in biochars. Based on previous research showing reduced hydrophobicity of soil with increasing water content [26], we hypothesized (4) that biochars exposed to air saturated with moisture (100% relative humidity) would take up more water than biochars kept at ambient relative humidity.

2. Materials and methods

2.1. Biochar production

Biochars were produced from Hazelnut shells (*Corylus avellana*; HZ) and Douglas-fir chips (*Pseudotsuga menziesii*; DF) under oxygen limited conditions using a prototype batch feed, slow pyrolysis retort with temperature monitoring and control capabilities. Both feedstocks are widely available waste products in Western Oregon. Hazelnut shells were purchased as cracked half shells without any portion of the nut remaining. Douglas-fir chips were supplied by Thompson Timber in Philomath, Oregon ($44^\circ 32' 37''$ N, $123^\circ 21' 52''$ W) and were produced from scrap log sections, excluding branches, bark, and leaves. The Douglas-fir chips had final dimensions of approximately $7 \text{ cm} \times 7 \text{ cm} \times 3 \text{ cm}$. Both feedstocks were stored in an open air environment prior to pyrolysis. Highest treatment temperatures (HTT) of 370°C , 500°C , and 620°C were selected to span known transitions in biochar properties [4]. Biochars were maintained at HTT for approximately 1 h. The time

spend in the retort, including ramp up and ramp down, was approximately 3 h. The six biochar products will be referred to as HZ 370, HZ 500, HZ 620, DF 370, DF 500, and DF 620.

2.2. Physical and chemical properties

Fixed carbon, ash content, and volatile matter were determined by proximate analysis via ASTM Method D 1762-84 [27]. N₂ adsorption data were collected in the range 0.1–0.3 P/P₀ using a Nova 2200e Surface Area Analyzer (Quantachrome, Boynton Beach, FL) to calculate multipoint BET-N₂ specific surface areas (m² g⁻¹). Prior to analysis, all samples were degassed for 18 h under vacuum at 150 °C. Volumetric surface area (m² cm⁻³) corresponds to the surface area per unit volume of biochar samples and was obtained by multiplying specific surface area (m² g⁻¹) by bulk density (g cm⁻³). Bulk density was determined by dividing sample mass by sample volume of packed cores described in Section 2.4. Solid density (g cm⁻³) was analyzed by helium pycnometry using a Quantachrome (Boynton Beach, FL) UltraPyc 1200e. The following equation was used to calculate porosity using pycnometry data: $\emptyset = 1 - D_b/D_p$, where \emptyset is porosity (volume fraction), D_b is bulk density (g cm⁻³), and D_p is solid density (g cm⁻³) determined by pycnometry.

2.3. PAS-FTIR

Photoacoustic Fourier Transform Infrared Spectroscopy (PAS-FTIR) was performed using a Thermo Nicolet Nexus 670 FT-IR spectrophotometer equipped with a photoacoustic accessory (MTEC Photoacoustics, Inc., Ames, IA) to investigate the chemical nature of biochar surfaces. PAS-FTIR was chosen instead of other FTIR methods due to the fact that the acoustic signal returned by PAS-FTIR is dominated by sample surface characteristics, therefore, results using PAS-FTIR primarily reflect functional groups located on, or in close proximity to biochar surfaces. Peak areas were calculated by subtracting linear regional baselines from smoothed data using PeakFit 4.12 (SeaSolve Software, Framingham, MA). Additional details of PAS-FTIR methods are included in Supporting Information.

2.4. Water and ethanol uptake experiments

Sub-samples of each biochar were ground and sieved to obtain the 125–500 μm size fraction for water and ethanol uptake experiments. Eight replicate samples of each ground biochar ($n = 8 \times 6$ biochars = 48) were packed into 3.2 cm tall cores made from 3 cm i.d. PVC pipe using a standard weight packing protocol. Additional details regarding the packing protocol are included in Supporting Information. Cloth coverings and rubber bands held biochar on both ends of PVC cores. After samples were packed, four replicates of each biochar were exposed to the ambient laboratory atmosphere for 8 days while the other four replicates were placed in a sealed chamber at 100% relative humidity for 8 days. Humidity pretreated samples were weighed periodically during the treatment and all samples were weighed on the eighth day at the completion of pretreatments. All samples were then submerged in water just to the top of each core in individual sample cups. Empty cores served as blanks to correct for water

held in cloth coverings. Each sample cup contained approximately 100 ml of water and 6–14 g of biochar, depending on biochar density. Samples were weighed after being allowed to drain freely on a wire mesh above sample cups for 60 s. Samples were replaced in the same sample cup and the water level in each cup was adjusted to rise just to the top of the sample core after each measurement. Fig. S-2 shows sample core construction, sample cup, and wire mesh for draining samples. Core weights were determined hourly during the first 8 h, then periodically for 18 days. Electrical conductivity (EC) and pH of sample cup water were measured using CON 700 EC meter (Oakton, Vernon Hills, IL) and a Basic AB15 pH meter (Accumet, Hudson, MA), respectively, following the 18 day water uptake experiment prior to discarding the water. Samples were decanted, dried at 65 °C for 10 days, and then weighed to determine dry mass and bulk density. 65 °C was used as the drying temperature instead of 105 °C to avoid melting PVC cores. Water content (volume fraction, %) was calculated for each time measurement after correcting for sample core tare weight and water held in cloth coverings. Water density was assumed to be 0.998 g cm⁻³ and sample volume was calculated as 22.7 cm³ from linear measurements of PVC cores.

After drying, the same samples were submerged in ethanol and weighed on a similar schedule using the same protocol as for water. Volumetric ethanol content (volume fraction, %) was calculated from ethanol uptake measurements with ethanol density assumed to be 0.789 g cm⁻³. Volumetric ethanol content was assumed to have reached equilibrium for all samples after approximately 500 h, after which time little change was noted in mass for any of the samples. Air-filled porosity (volume fraction, %) of water-wet samples was calculated by subtracting water content from total porosity calculated using pycnometry data. Water saturation is the fraction of total pore volume (%) occupied by water and was calculated by dividing water content by the total porosity value derived from pycnometry data.

2.5. Statistical analysis

Between-group differences in final water content, final ethanol content, water saturation, and air filled porosity were analyzed for statistical significance using 1-way ANOVA with Tukey pair-wise comparisons at the 0.05 significance level. The specific effects of feedstock and production temperature on final water content, final ethanol content, and water saturation were assessed using two-way ANOVA. Porosity values determined by ethanol uptake were compared to pycnometry derived porosity values using a two-tailed paired t-test. Normality and equality of variances were confirmed prior to each statistical analysis.

3. Results and discussion

3.1. Basic properties

Proximate analysis, pH, and electrical conductivity data follow previously reported trends indicating loss of volatile compounds, relative enrichment in ash content, and conversion of

a portion of remaining carbon compounds into fixed carbon with increasing production temperatures [6]. All biochar samples had a pH of 7.6 or greater, with higher pH exhibited by higher temperature biochars (Table S-1), following previously reported data [9,28]. Likewise, electrical conductivity generally increased with increasing production temperature with the exception of slight declines from DF 370 to DF 500 and from HZ 500 to HZ 620. Fixed carbon, volatile matter, and ash content were similar between feedstocks, with greater fixed carbon and lower volatile matter noted for higher temperature biochars (Table S-1). Ash content increased with production temperature in DF biochars but did not notably increase in HZ biochars with increasing production temperatures. Additional discussion of basic properties is included in Supporting Information.

3.2. PAS-FTIR

PAS-FTIR spectra (Fig. 1) show decreasing surface functionality in higher production temperature biochars for both feedstocks. Peak area estimates confirm this trend (Table S-2), with both the C–H/CH₃ aliphatic peak (wavenumber 2800–2990 cm⁻¹) and the C=O region (wavenumber 1680–1730 cm⁻¹) decreasing in area with increasing production temperature. The C–H/CH₃ aliphatic peak is of interest as it has recently been positively correlated with hydrophobicity in biochars [29]. The C=O peak is of interest as it primarily represents ionisable carboxyl groups and would therefore identify hydrophilic surface functionality. In general, PAS-FTIR results are similar to previously reported FTIR data using Attenuated Total Reflectance (ATR) [29,30] and PAS [28],

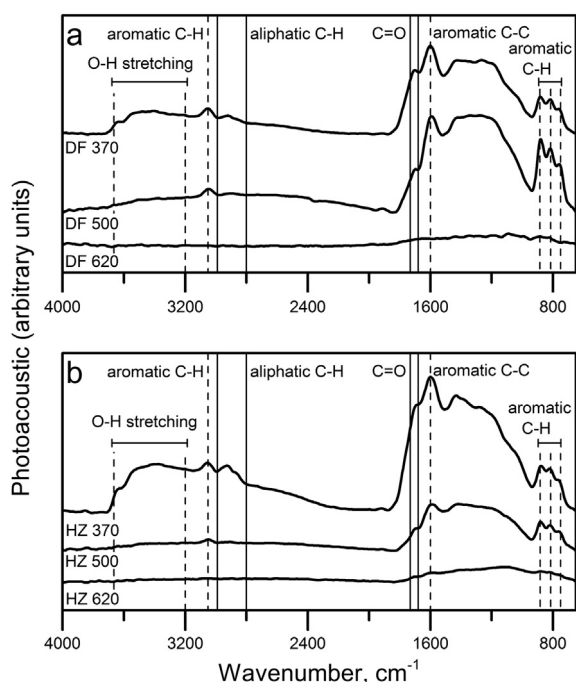


Fig. 1 – Sample PAS-FTIR spectra for Douglas fir (a) and hazelnut shell (b) chars produced at 300 °C, 500 °C, and 620 °C. Solid bars delineate aliphatic C–H (2800–2990) and C=O (1680–1730) regions used in peak area estimates (see Table S-2).

and indicate diminishing functional group abundance and diversity with increasing production temperature.

3.3. Physical properties

Specific surface area was greater in DF biochars than in HZ biochars and increased with production temperature, while volumetric surface area also increased with production temperature, but was generally greater in HZ biochars than in DF biochars (Table 1). The positive correlation between surface area and production temperature has been widely reported and is explained by Kercher and Nagle [3] as the result of condensation of carbon into denser turbostratic crystallites leaving nanometer-sized voids (pyrogenic nanopores) within the carbon structure. Volumetric surface areas of 40.2 m² cm⁻³ and 32.6 m² cm⁻³ in DF 370 and HZ 370 biochars, respectively, indicate some limited pyrogenic nanopore formation even in low temperature biochars, as these values cannot be accounted for by residual macroporosity alone. Particle density was similar between feedstocks and slightly greater for higher temperature biochars (Table 1), with results similar to previously published data [3,18]. Both porosity methods (ethanol uptake and pycnometry) showed approximately 20% greater porosity in DF biochars compared to HZ biochars (Table 1), which explains the greater bulk density of HZ biochars compared to DF biochars. Given that all samples were ground to retain only the 125–500 μm size fraction, external porosity can be considered constant between all samples, implying that differences in total porosity between feedstocks indicate greater internal porosity in DF biochars compared to HZ biochars. Because these differences are noted even for 370 °C biochars, which contain only limited pyrogenic nanopore formation [19], DF biochars must contain greater residual macropore volume than HZ biochars.

As noted, porosity increased only slightly with increasing production temperature (as calculated by pycnometry data). Assuming consistent external pore volume across all samples, these results indicate that internal pore volume (i.e., the sum of pyrogenic nanoporosity and residual macroporosity) increases only slightly with increasing production temperature. Haas et al. [31] visually estimated the cross-sectional area of residual macropores in slices of poplar during fast pyrolysis (150 °C min⁻¹) between 50 °C and 550 °C, and observed rapidly increasing cross-sectional pore areas between 350 °C and 450 °C, but no increase in cross-sectional pore area above approximately 450 °C. Rapid increases in cross-sectional pore area between 350 °C and 450 °C were attributed to loss of liquid and gaseous products due to thermal decomposition of lignocellulosic material. Keiluweit et al. [4] similarly noted rapid loss of volatile matter in grass and pine biochars between 300 °C and 400 °C with less volatile matter lost above this region, and proposed that this temperature region marks the transition from relatively unaltered feedstock compounds to amorphous, thermally-altered biochars. Constant cross-sectional pore area above 450 °C noted by Haas et al. [31] suggests that residual macropore volume reaches a relatively stable level above some temperature threshold, which may coincide with the end of the transition char region proposed by Keiluweit et al. [4]. Because the majority of internal pore volume exists in residual macropores [15], the fact that production temperature had

Table 1 – Biochar bulk density, specific surface area, volumetric surface area, particle density, and porosity calculated by both pycnometry data and measured by ethanol uptake for Douglas fir and hazelnut shell chars produced at 370 °C, 500 °C, and 620 °C.

Feedstock	Pyrolysis temperature	Bulk density ^a	Specific surface area	Volumetric surface area	Particle density (pycnometry)	Porosity (pycnometry)	Porosity (ethanol)
	°C	g cm ⁻³	m ² g ⁻¹	m ² cm ⁻³	g cm ⁻³	Volume fraction (%)	Volume fraction (%)
Douglas fir	370	0.262 ± 0.005	153 ± 4.7	40.2 ± 1.4	1.55 ± 0.01	83.0 ± 0.3	86.3 ± 0.8
	500	0.236 ± 0.007	229 ± 4.9	54.2 ± 2.1	1.57 ± 0.04	84.9 ± 0.5	88.2 ± 0.3
	620	0.254 ± 0.010	280 ± 9.7	71.1 ± 3.7	1.71 ± 0.02	85.1 ± 0.6	86.7 ± 1.0
Hazelnut shell	370	0.554 ± 0.007	58.7 ± 7.1	32.6 ± 3.9	1.48 ± 0.04	62.5 ± 0.4	66.6 ± 0.4
	500	0.557 ± 0.009	161 ± 1.1	89.5 ± 1.6	1.57 ± 0.01	64.5 ± 0.6	65.4 ± 0.9
	620	0.505 ± 0.005	211 ± 5.0	106 ± 2.8	1.64 ± 0.01	69.2 ± 0.3	68.0 ± 0.3

Values following ± indicate standard error.

^a Bulk Density values are for packed sample cores.

little effect on total pore volume in our biochars suggests that our biochars had proceeded through the transition char region and achieved relatively stable residual macroporosity, at lower temperatures than the 450 °C threshold reported by Haas et al. [31]. This discrepancy in threshold temperature could be explained by the slower heating rates and longer hold times used in the production of our biochars compared to the rapid charring done by Haas et al. [31]. Given constant residual macroporosity across the range of production temperatures, the slight increases in porosity (as calculated by pycnometry data) with greater production temperature (Table 1) may indicate an increase in pyrogenic nanoporosity rather than any change in residual macroporosity.

When surface area is considered on a volumetric basis (Table 1), we find the largest values in high temperature HZ biochars. Given that the majority of surface area is found in pyrogenic nanopores [19], higher volumetric surface area and lower total porosity in HZ 620 biochars compared to DF 620 biochars (Table 1) suggests greater pyrogenic nanopore formation (on a volumetric basis) in HZ 620 biochars compared to DF 620 biochars. If all pyrogenic nanopores form within the solid biochar volume (non-pore space), we can see from total porosity data that HZ 370 and DF 370 samples contain 38% and 17% solid biochar volume, respectively, available for pyrogenic nanopore formation. This explains the greater increase in porosity (6.7% vs. 2.1%) as well as the greater increase in volumetric surface area (73.8 m² cm⁻³ vs. 30.9 m² cm⁻³) observed in HZ biochars compared to DF biochars from 370 °C to 620 °C production temperature (Table 1). These trends suggest that initially less porous feedstocks have the potential to develop greater surface area and pyrogenic nanoporosity on a per volume basis than initially more porous feedstocks.

While total porosity remained relatively stable with increasing production temperature, pyrogenic nanoporosity is known to increase dramatically between 370 °C and 620 °C [15], suggesting that these pores constitute only a small portion of total porosity. To illustrate this phenomenon, we propose a physical pore model (Fig. 2) with 3 basic components: 1) stable residual macroporosity based on plant cellular structure and independent of production temperature above a certain temperature threshold; 2) pyrogenic nanoporosity that develops within the solid biochar volume and increases rapidly with

production temperature but constitutes only a small portion of total porosity, even in higher production temperature biochars; and 3) aliphatic functionality on residual macropore walls that becomes volatilized and lost at higher production temperatures, according to PAS-FTIR data (Fig. 1) and visual observations [31]. The model presented in Fig. 2 is intended to represent a cross section of softwood biochar based on numerous SEM images [13] and standard microscopy [31], and does not include interparticle or external porosity. HZ biochars and biochars from other feedstocks would exhibit different residual macropore structures; however, these biochars are expected to follow this model with increasing production temperature. This model does not incorporate dimensional shrinkage of the biochar matrix, which has been observed by several research groups [3,13,31]. Total dimensional shrinkage between 370 °C and 620 °C would be on the order of 10–20% [3], and could reduce the total volume available for pyrogenic nanopore formation in higher temperature biochars, but would not substantially affect the proposed physical pore model.

Using this model and assuming limited pyrogenic nanoporosity in 370 °C biochars, increases in total porosity from 370 °C to 620 °C production temperature (Table 1) indicate that pyrogenic nanopores account for approximately 2.1% and 6.7% of total biochar volume for DF 620 and HZ 620 biochars, respectively. Although previous research has reported substantial increases in total porosity with increasing production temperature due to pyrogenic nanopore formation [15,16,19], these research groups characterized total pore volume by N₂ adsorption at 77 K, which only measures volume accurately in pores smaller than 50 nm [12]. This method excludes external pores, which can amount to greater than 50% of total pore volume in sand-sized porous media (similar to size fraction used here) depending on compaction, and residual macropores. The methods presented here account for the entire porosity of granular biochar as a packed porous medium, of which pores smaller than 50 nm constitute only a fraction. Thus, while pyrogenic nanoporosity increases substantially with increasing production temperature, the contribution to total porosity of biochar as a packed porous medium is quite small.

Porosity determined by ethanol uptake was similar to porosity calculated using pycnometry data, however, with increasing production temperature, porosity increased

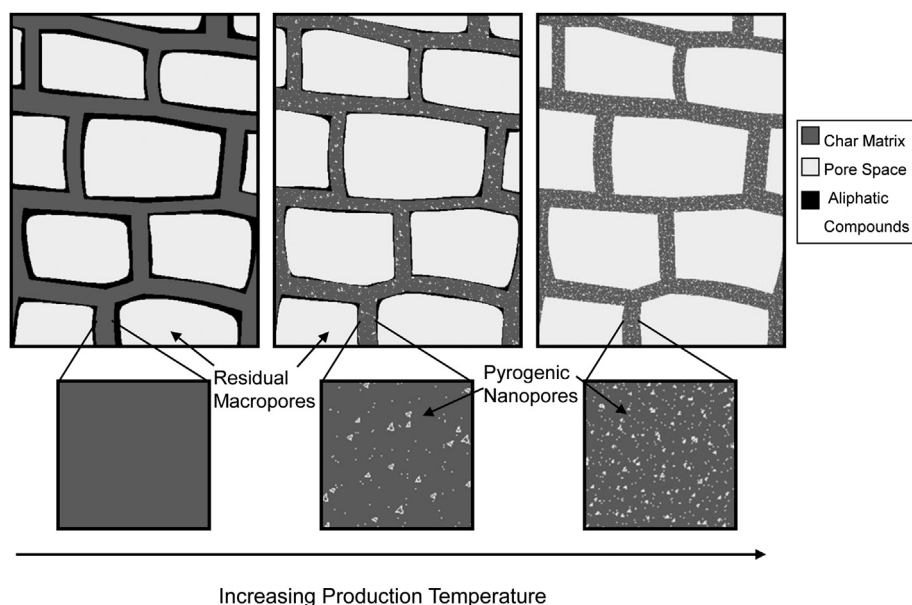


Fig. 2 – Physical pore model illustrating residual macroporosity, pyrogenic nanoporosity, and aliphatic compounds across a production temperature gradient. Magnification boxes depict evolution of pyrogenic nanoporosity with increasing production temperature.

slightly when calculated using pycnometry data, but did not increase when measured by ethanol uptake (Table 1). A two-sided paired t-test indicated that results were statistically different ($p < 0.001$) with a mean porosity difference of 1.95% between the two methods (95% CI: 1.15%–2.69% porosity). Greater porosity measured by ethanol uptake may be due to slight bulging of the cloth core ends when submerged in ethanol, allowing excess ethanol to be held beyond the measured core volume. This excess ethanol was not accounted for by blank cores, which only accounted for ethanol held in cloth coverings. Since ethanol molecules are larger than helium atoms, there may be a portion of pyrogenic nanoporosity not accessible or only partially accessible to ethanol that is more accessible to helium gas. This may explain why differences between the methods are larger for lower temperature biochars and smaller for higher temperature biochars: higher temperature biochars contain greater pyrogenic nanoporosity which would be less accessible to ethanol, partially offsetting the effect of bulging cores. It is thought that the pycnometry method provides more accurate results; however, with additional methodological refinement, the ethanol uptake may be a suitable low-cost alternative to pycnometry to determine porosity differences between biochars produced from different feedstocks.

3.4. Water and ethanol uptake

Water uptake curves (Fig. 3a) show greater uptake for DF biochars compared to HZ biochars and greater uptake for higher temperature biochars compared to lower temperature biochars. One-way ANOVA with subsequent Tukey pair-wise comparisons confirm that the final water content of each group was significantly different (at the $p < 0.05$ level) from every other group except for DF 500 and DF 620 (Table 2). Two-

way ANOVA analysis of final water content with feedstock and production temperature as factors indicated that both factors were significant at the $p < 0.05$ level. Water uptake rates for all biochars declined rapidly within the first 8 h, with rates converging after 4 h for each group except DF 500 (Fig. S-3). DF 500 samples maintained an elevated level of uptake through approximately 180 h as illustrated in Fig. 3a. All groups continued to take up water at the conclusion of the 21 day experiment at approximately the same rate. For each group, approximately half of the total 21 day water uptake occurred before the first measurement at 5 min after submersion (Table 2). These results indicate that water uptake depends on both feedstock selection and production temperature. Results from the 100% relative humidity pretreatment experiment are discussed in Supporting Information.

As opposed to water uptake, ethanol uptake (Fig. 3b) depended only on feedstock and not on production temperature, with DF samples taking up more ethanol than HZ samples. One-way ANOVA analysis with subsequent Tukey pair-wise comparisons of final ethanol uptake (Table 2) confirms greater ethanol uptake by DF biochars compared to HZ biochars; however, there was no difference in uptake across production temperatures within feedstocks. This was supported with two-way ANOVA analysis of ethanol uptake, which indicated that feedstock was a significant factor at the $p < 0.05$ level, but production temperature was not. Ethanol uptake was more rapid and more complete than water uptake, with rapid uptake during the first day followed by steadily declining uptake rates until equilibrium was reached after approximately 21 days (~500 h). Water saturation curves (Fig. 3c), which represent water uptake normalized to pore volume, are grouped primarily by production temperature, with HZ 620 samples attaining the greatest final saturation of 92.7% and HZ 370 samples attaining saturation of only 86.0% (Table 2). Two-way ANOVA analysis of

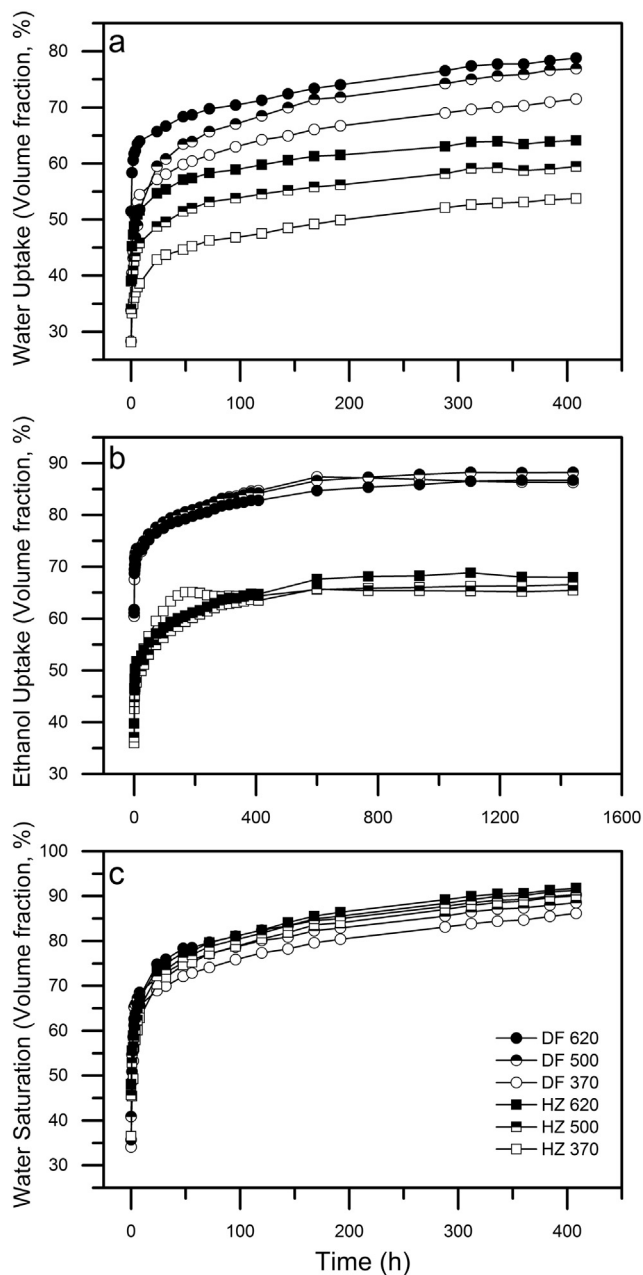


Fig. 3 – Water uptake (a), ethanol uptake (b), and water saturation (c) for Douglas fir and hazelnut shell chars produced at 370 °C, 500 °C, and 620 °C production temperature.

water saturation with feedstock and production temperature as factors indicated that only production temperature was a significant factor at the $p < 0.05$ level. Final air-filled porosity was greater for lower temperature biochars and greater for DF compared to HZ biochars (Table 2), with a maximum mean value of 11.5% noted in DF 370 samples.

3.5. Effects of porosity versus effects of hydrophobicity

Water and ethanol uptake experiments yielded fundamentally different results: water uptake was dependent on both

feedstock and production temperature; however, ethanol uptake was dependent only on feedstock (Table 2). Since ethanol is assumed to be a fully-wetting liquid with a zero-degree contact angle on most surfaces, it would be subject only to positive capillary forces, which enhance uptake into pores. Therefore, ethanol would saturate nearly all biochar porosity. The fact that ethanol uptake was not dependent on production temperature indicates no difference in liquid accessible porosity between different production temperature biochars. Water, on the other hand, is subject to both positive and negative capillary forces, depending on biochar surface hydrophobicity. Therefore, differences in water uptake between different production temperature biochars must be attributed to non-porosity factors. This is illustrated by water saturation, indicating greater saturation in higher temperature biochars (Fig. 3c, Table 2). These differences can only be explained by non-porosity factors such as pressurized pore air, pyrogenic nanopore blockage by tars and oils, or hydrophobicity, since water saturation values are already normalized for porosity values calculated using pycnometry data. Neither oxygen nor nitrogen is highly soluble in water [24,25], so water intrusion into “dead-end” pores would cause an increase in air pressure that could prevent further intrusion of water into these pores. This effect would likely occur primarily in “dead-end” pyrogenic nanopores, which are more abundant in higher temperature biochars. Thus, pressurized pore air may partially explain why none of the biochars reached 100% water saturation (Table 2), but it does not explain why higher temperature biochars took up more water than lower temperature chars. Pyrogenic nanopore blockage by condensed oils has been reported in lower temperature biochars [13]. However, since differences in water uptake were noted during the first 5 min of submersion (Table 2) when pyrogenic nanopore filling would be minimal, we do not consider pyrogenic nanopore blockage to be a major factor in differences of water uptake. Both pressurized pore air and pyrogenic nanopore blockage would preferentially reduce water uptake in higher temperature biochars. Since our water uptake data show greater uptake by higher temperature biochars, surface hydrophobicity and resultant capillary forces must account for these differences.

Aliphatic surface functionality detected using FTIR (Fig. 1, Table S-2) may explain differences in hydrophobicity between samples, as proposed by Kinney et al. [29]. Novak et al. [32] also suggested reduced hydrophobicity in higher temperature biochars could be due to changes in the proportions of hydrophobic and hydrophilic functional groups, but did not specifically identify aliphatic groups. The presence of the aliphatic peak ($2800\text{--}2990\text{ cm}^{-1}$) is thought to indicate residual aliphatic compounds that are volatilized at higher production temperatures [33]. This aliphatic peak may also represent pyrogenic tars and oils that are unable to escape the biochar matrix during pyrolysis [31]. Aliphatic compounds on biochar surfaces, as depicted in the physical pore model (Fig. 2), would render these surfaces hydrophobic, creating negative capillary forces of considerable magnitude in pyrogenic nanopores and residual macropores (Equation (1)), effectively preventing water entry in these pores under standard, non-pressurized conditions. Because all biochar surfaces are inherently located within pores (Fig. S-1), the relative

Table 2 – Final vapor uptake, 5-minute water uptake, final water uptake, final ethanol uptake, water saturation, and final air-filled porosity for Douglas fir and hazelnut shell chars produced at 370 °C, 500 °C, and 620 °C.

Feedstock	Production temperature	Vapor uptake ^{a,b}	5-min water uptake ^b	Mean water uptake	Mean ethanol uptake	Mean water saturation	Mean air filled porosity
	°C	Volume fraction (%)	Volume fraction (%)	Volume fraction (%)	Volume fraction (%)	Volume fraction (%)	Volume fraction (%)
Douglas fir	370	2.32 ± 0.10	28.3 ± 6.4	71.5d	86.3b	86.1a	11.5b
	500	2.55 ± 0.16	33.8 ± 10.5	76.9e	88.2b	90.6 ab	8.0 ab
	620	2.94 ± 0.23	51.5 ± 1.6	78.8e	86.7b	92.6b	6.3a
Hazelnut shell	370	3.90 ± 0.03	28.2 ± 2.6	53.8a	66.6a	86.0a	8.7 ab
	500	5.33 ± 0.15	34.1 ± 1.4	59.4b	65.4a	92.1b	5.1a
	620	6.26 ± 0.09	39.0 ± 1.6	64.1c	68.0a	92.7b	5.1a

Means followed by the same letter within a column are not statistically different at $p < 0.05$ using a Tukey HSD pair-wise comparison following ANOVA.

Values following ± indicate standard error.

^a Vapor uptake data only for 100% RH treated samples.

^b vapor uptake and 5-minute water uptake not analyzed using ANOVA due to sample heteroskedasticity.

location of aliphatic compounds in different pore types would affect only the magnitude of negative capillary forces, not the presence or absence of such forces. The presence of aliphatic compounds on surfaces in external pores would generate negative capillary forces of only modest magnitude. Given that all biochar samples achieved water saturation greater than 80% (Table 2), hydrophobic aliphatic compounds are likely found only in a portion of biochar pores. Indeed, because all samples were ground and sieved after pyrolysis, it is expected that a large portion of biochar surfaces located in external pores were created during grinding, and would be less likely to contain condensed or residual aliphatic compounds, as these surfaces were not present during pyrolysis. Volatilization and loss of these compounds during pyrolysis at higher temperatures would cause biochar surfaces to become less hydrophobic or even exhibit hydrophilic tendencies, causing capillary forces to enhance, rather than prevent, water entry into pores. It is not clear whether this reduction in hydrophobicity occurs uniformly in all pores, or whether certain pores remain hydrophobic when volatilized compounds are unable to escape during pyrolysis, as observed by Haas et al. [31]. Higher production temperatures, longer reactor hold times, and smaller feedstock particle sizes may aid in the removal of these compounds from biochar.

3.6. Pore filling by vapor sorption and liquid water uptake

Water vapor sorption literature indicates that micropore filling by water vapor occurs at high relative humidity in both activated carbons [34] and biochars [35]. This phenomenon is thought to occur by sorption of individual water molecules onto polar surface functional groups, followed by molecular cluster formation and growth, and subsequent pore filling [34]. Pastor-Villegas et al. [35] investigated water vapor sorption in biochars produced between 250 °C and 1000 °C and determined that all micropores (<2 nm) were completely filled by water vapor above a relative humidity of 95%, with some mesopore (2–50 nm) filling between 95% and 100% relative humidity. When our biochars were submerged in liquid water, air-filled pores within our biochars would have been at 100%

relative humidity, so pore filling by water vapor would be expected in pyrogenic nanopores (primarily smaller than 2 nm) regardless of the ability of liquid water to fill these pores. Indeed, when we monitored water vapor sorption during the 100% relative humidity pretreatment, we found greater water vapor sorption in higher temperature biochars (Table 2) which contain greater pyrogenic nanoporosity, confirming that vapor sorption occurred in at least a portion of these pores. Pyrogenic nanopores are particularly important for aqueous contaminant sorption, which requires saturation and hydraulic connectivity of these pores as they are thought to be the primary sorption sites in biochars [7,19].

Given that uptake of water vapor during the humidity pretreatment was complete after 7 days, we may assume that filling of small pyrogenic nanopores by water vapor is complete after 7 days. Therefore, steady water uptake after 7 days (168 h, Fig. 3a) must be attributed to filling of external pores, residual macropores, and those larger pyrogenic nanopores not filled by water vapor sorption. This persistent water uptake may be due to decreasing surface hydrophobicity with increasing moisture content within pores [26]. Oxidation has also been reported in moist biochars during incubation experiments [36] and could render biochar surfaces less hydrophobic by increasing the abundance of oxygen-containing functional groups. This may be partially responsible for continued water uptake in our biochars and would be expected to continue beyond the end of the experiment. Continued water uptake due to either proposed mechanism implies that hydrophobicity in biochars may not be a concern for longer-term biochar applications that remain saturated.

4. Conclusions

Our results indicate that water uptake by biochars is dependent on both feedstock selection, which controls residual macroporosity, and production temperature, which controls hydrophobicity and pyrogenic nanopore formation. With increasing production temperature, residual macroporosity remains relatively constant while pyrogenic nanoporosity increases dramatically. Under the sample packing procedures

used in this study, total porosity was composed primarily of external pores and residual macropores. Pyrogenic nanopores contributed only minimally to total porosity, even in higher temperature biochars, but these pores provide the majority of biochar surface area critical for contaminant and nutrient sorption. Saturation of pores depends on surface chemistry, which can render biochar surfaces hydrophobic, creating negative capillary pressure that prevents water from entering pores. Overall, hydrophobicity in biochars decreased with increasing production temperature and may be due to aliphatic functionality which is volatilized and lost at higher production temperatures. Reducing particle size and increasing production hold times may also help reduce hydrophobicity by allowing greater loss of hydrophobic compounds from biochar particles during pyrolysis. Hydrophobicity is most relevant in external pores and residual macropores, as pyrogenic nanopores likely fill by water vapor sorption when biochars are submerged in water.

This work shows that production of effective “designer biochars” for water retention applications requires careful selection of feedstock and production temperature to produce suitable products. Production of biochars for filtration applications requiring sorption of contaminants in pyrogenic nanopores requires additional considerations to ensure adequate volume and hydraulic connectivity of these pores. Our research indicates that initially less porous feedstocks have the ability to evolve greater pyrogenic nanoporosity at high production temperatures, meaning that these biochars may be preferable for filtration applications. Biochars made from carbon-rich, small particle size feedstocks produced at high production temperatures with long hold time are likely to provide optimal properties for both water retention and filtration applications. However, carbon-rich feedstocks are more expensive, and finer feedstock grinding, higher production temperatures, and longer hold times each add cost to the production process. Thus, production of “designer biochars” for water retention and filtration applications requires careful optimization to achieve adequate performance using available feedstocks at economically feasible costs.

Acknowledgments

This research was supported by grants from the Western Regional Center of the Sun Grant Initiative and from the Agricultural Research Foundation at Oregon State University. MK further acknowledges support through a research fellowship from the Institute of Soil Landscape Research, Leibniz—Center for Agricultural Landscape Research (ZALF), 15374 Muencheberg, Germany. The authors appreciate usage of analytical equipment at US Environmental Protection Agency in Corvallis, OR. The authors are also grateful to John Miedema of Biological Carbon who produced the biochars used in this study. The information in this document has been funded in part by the U.S. Environmental Protection Agency. It has been subjected to review by the National Health and Environmental Effects Research Laboratory’s Western Ecology Division and approved for publication. Approval does not signify that the contents reflect the views of the Agency, nor

does mention of trade names or commercial products constitute endorsement or recommendation for use.

Appendix A. Supplementary data

Supplementary data related to this article can be found at <http://dx.doi.org/10.1016/j.biombioe.2013.12.010>.

REFERENCES

- [1] Lehmann J. Bio-energy in the black. *Front Ecol Environ* 2007;5(7):381–7.
- [2] Laird DA, Brown RC, Amonette JE, Lehmann J. Review of the pyrolysis platform for coproducing bio-oil and biochar. *Biofuel Bioprod Bior* 2009;3(5):547–62.
- [3] Kercher AK, Nagle DC. Microstructural evolution during charcoal carbonization by X-ray diffraction analysis. *Carbon* 2003;41(1):15–27.
- [4] Keiluweit M, Nico PS, Johnson MG, Kleber M. Dynamic molecular structure of plant biomass-derived black carbon (biochar). *Environ Sci Technol* 2010;44(4):1247–53.
- [5] Glaser B, Lehmann J, Zech W. Ameliorating physical and chemical properties of highly weathered soils in the tropics with charcoal – a review. *Biol Fert Soils* 2002;35(4):219–30.
- [6] Antal MJ, Grønli M. The art, science, and technology of charcoal production. *Ind Eng Chem Res* 2003;42(8):1619–40.
- [7] Chun Y, Sheng G, Chiou CT, Xing B. Compositions and sorptive properties of crop residue-derived chars. *Environ Sci Technol* 2004;38(17):4649–55.
- [8] Rutherford DW, Wershaw RL, Rostad CE, Kelly CN. Effect of formation conditions on biochars: compositional and structural properties of cellulose, lignin, and pine biochars. *Biomass Bioenergy* 2012;46:693–701.
- [9] Novak JM, Busscher WJ, Laird DL, Ahmedna M, Watts DW, Niandou MAS. Impact of biochar amendment on fertility of a southeastern coastal plain soil. *Soil Sci* 2009;174(2):105–12.
- [10] Uchimiya M, Lima IM, Klasson KT, Chang S, Wartelle LH, Rodgers JE. Immobilization of Heavy metal ions (Cu-II, Cd-II, Ni-II, and Pb-II) by broiler litter-derived biochars in water and soil. *J Agr Food Chem* 2010;58(9):5538–44.
- [11] Tsui L, Roy WR. The potential applications of using compost chars for removing the hydrophobic herbicide atrazine from solution. *Bioresour Technol* 2008;99(13):5673–8.
- [12] Rouquerol J, Avnir D, Fairbridge CW, Everett DH, Haynes JM, Pernicone N, et al. Recommendations for the characterization of porous solids (Technical Report). *Pure Appl Chem* 1994;66(8):1739–58.
- [13] Pulido-Novicio L, Hata T, Kurimoto Y, Doi S, Ishihara S, Imamura Y. Adsorption capacities and related characteristics of wood charcoals carbonized using a one-step or two-step process. *J Wood Sci* 2001;47(1):48–57.
- [14] Wildman J, Derbyshire F. Origins and functions of macroporosity in activated carbons from coal and wood precursors. *Fuel* 1991;70(5):655–61.
- [15] Sun H, Hockaday WC, Masiello CA, Zygourakis K. Multiple controls on the chemical and physical structure of biochars. *Ind Eng Chem Res* 2012;51(9):3587–97.
- [16] Bornemann LC, Kookana RS, Welp G. Differential sorption behavior of aromatic hydrocarbons on charcoals prepared at different temperatures from grass and wood. *Chemosphere* 2007;67(5):1033–42.
- [17] Zhu D, Kwon S, Pignatello JJ. Adsorption of single-ring organic compounds to wood charcoals prepared under

- different thermochemical conditions. *Environ Sci Technol* 2005;39(11):3990–8.
- [18] Fu P, Hu S, Xiang J, Sun L, Su S, Wang J. Evaluation of the porous structure development of chars from pyrolysis of rice straw: effects of pyrolysis temperature and heating rate. *J Anal Appl Pyrol* 2012;98:177–83.
- [19] Li W, Yang K, Peng J, Zhang L, Guo S, Xia H. Effects of carbonization temperatures on characteristics of porosity in coconut shell chars and activated carbons derived from carbonized coconut shell chars. *Ind Crop Prod* 2008;28(2):190–8.
- [20] Brockhoff SR, Christians NE, Killorn RJ, Horton R, Davis DD. Physical and mineral-nutrition properties of sand-based turfgrass root zones amended with biochar. *Agron J* 2010;102(6):1627.
- [21] Klose W, Schinkel A. Measurement and modelling of the development of pore size distribution of wood during pyrolysis. *Fuel Process Technol* 2002;77-78:459–66.
- [22] Baldock JA, Smernik RJ. Chemical composition and bioavailability of thermally altered *Pinus resinosa* (Red pine) wood. *Org Geochem* 2002;33(9):1093–109.
- [23] Watson CL, Letey J. Indices for characterizing soil-water repellency based upon contact angle-surface tension relationships. *Soil Sci Soc Am J* 1970;34(6):841–4.
- [24] Battino R, Rettich T, Tominaga T. The solubility of oxygen and ozone in liquids. *J Phys Chem Ref Data* 1983;12(2):163–78.
- [25] Battino R, Rettich T, Tominaga T. The solubility of nitrogen and air in liquids. *J Phys Chem Ref Data* 1984;13(2):563–600.
- [26] Liu H, Ju Z, Bachmann J, Horton R, Ren T. Moisture-dependent wettability of artificial hydrophobic soils and its relevance for soil water desorption curves. *Soil Sci Soc Am J* 2012;76(2):342–9.
- [27] ASTM. Standard test method for chemical analysis of Wood charcoal D2762-84(2013). West Conshohocken, PA (USA): American Society for Testing and Materials; 2013.
- [28] Yuan J-H, Xu R-K, Zhang H. The forms of alkalis in the biochar produced from crop residues at different temperatures. *Bioresour Technol* 2011;102(3):3488–97.
- [29] Kinney TJ, Masiello CA, Dugan B, Hockaday WC, Dean MR, Zygourakis K, et al. Hydrologic properties of biochars produced at different temperatures. *Biomass Bioenergy* 2012;41:34–43.
- [30] Cantrell KB, Hunt PG, Uchimiya M, Novak JM, Ro KS. Impact of pyrolysis temperature and manure source on physicochemical characteristics of biochar. *Bioresour Technol* 2012;107:419–28.
- [31] Haas TJ, Nimlos MR, Donohoe BS. Real-time and post-reaction microscopic structural analysis of biomass undergoing pyrolysis. *Energ Fuel* 2009;23(7):3810–7.
- [32] Novak JM, Busscher WJ, Watts DW, Amonette JE, Ippolito JA, Lima IM, et al. Biochars impact on soil-moisture storage in an ultisol and two aridisols. *Soil Sci* 2012;177(5):310–20.
- [33] Chen B, Zhou D, Zhu L. Transitional adsorption and partition of nonpolar and polar aromatic contaminants by biochars of pine needles with different pyrolytic temperatures. *Environ Sci Technol* 2008;42(14):5137–43.
- [34] Brennan JK, Bandosz TJ, Thomson KT, Gubbins KE. Water in porous carbons. *Colloid Surf A* 2001;187–188:539–68.
- [35] Pastor-Villegas J, Meneses Rodriguez JM, Pastor-Valle JF, Rouquerol J, Denoyel R, Garcia Garcia M. Adsorption-desorption of water vapour on chars prepared from commercial wood charcoals, in relation to their chemical composition, surface chemistry and pore structure. *J Anal Appl Pyrol* 2010;88(2):124–33.
- [36] Zimmerman AR. Abiotic and microbial oxidation of laboratory-produced black carbon (biochar). *Environ Sci Technol* 2010;44(4):1295–301.